Combined Visualization and Heat Transfer Measurements for Steam Flow Condensation in Hydrophilic and Hydrophobic Mini-Gaps

Xi Chen
Department of Mechanical and Nuclear Engineering,
Kansas State University,
Manhattan, KS 66506

Melanie M. Derby[1]
Department of Mechanical and Nuclear Engineering,
Kansas State University,
Manhattan, KS 66506
e-mail: derbym@ksu.edu

*Condensation enhancement was investigated for flow condensation in mini-channels. Simultaneous flow visualization and heat transfer experiments were conducted in 0.952-mm diameter mini-gaps. An open loop steam apparatus was constructed for a mass flux range of 50–100 kg/m^{2}s and steam quality range of 0.2–0.8, and validated with single-phase experiments. Filmwise condensation was observed in the hydrophilic mini-gap; pressure drop and heat transfer coefficients were compared to the (Kim and Mudawar, 2013, "Universal Approach to Predicting Heat Transfer Coefficient for Condensing Mini/Micro-Channel Flow," Int. J. Heat Mass Transfer, **56**(1–2), pp. 238–250) correlation and prediction was very good; the mean absolute error (MAE) was 20.2%. Dropwise condensation was observed in the hydrophobic mini-gap, and periodic cycles of droplet nucleation, coalescence, and departure were found at all mass fluxes. Snapshots of six typical sweeping cycles were presented, including integrated flow visualization quantitative and qualitative results combined with heat transfer coefficients. With a fixed average steam quality ($\bar{x} = 0.42$), increasing mass flux from 50 to 75 to 100 kg/m^{2}s consequently reduced average sweeping periods from 28 to 23 to 17 ms and reduced droplet departure diameters from 13.7 to 12.9 to 10.3 μm, respectively. For these cases, condensation heat transfer coefficients increased from 154,700 to 176,500 to 194,800 W/m^2 K at mass fluxes of 50, 75, and 100 kg/m^2 s, respectively. Increased mass fluxes and steam quality reduced sweeping periods and droplet departure diameters, thereby reducing liquid thickness and increasing heat transfer coefficients.* [DOI: 10.1115/1.4033496]

1 Introduction

Condensers are critical heat exchangers for a wide range of applications, such as power plants, seawater desalination, and chemical processing equipment [1]. In 2014, 86% of electricity in the United States was generated using thermal cycles [2]. These thermal power plants are significant water users, and 544 power plants withdraw at least 2×10^6 gallons of cooling water every day [2]. Air-cooled condensers would greatly reduce water usage for power generation, but dry cooling is currently an expensive option [3]. Reductions in steam- and air-side thermal resistances in air-cooled condensers would yield more compact, economical condensers. For in-tube steam condensation, liquid-phase thermal resistance dominates condensation, and reduced liquid film thicknesses, such as those encountered in dropwise condensation, increase condensation heat transfer coefficients.

Internal flow condensation enhancements which reduce liquid film thickness, such as mini-channels and dropwise condensation, are the focus of this study. Compared to conventional-sized hydrophilic channels, hydrophilic mini-channels, and microchannels have been shown to enhance condensation heat transfer [4–8]. Kandlikar [9] considered mini-channels to have diameters between 200 μm and 3 mm and microchannels to have diameters between 10 μm and 200 μm. Flow regimes and subsequent heat transfer performance have also been shown to differ in mini-channels as compared to conventional channels, enhancing condensation heat transfer [10–12]. In mini- and microchannels, body forces such as gravity and buoyancy decrease in significance and surface tension increases in importance [10–15]. Condensation heat transfer coefficients typically increase with increasing mass flux and steam quality [7,8,12,13,16,17], except at low qualities [4,18].

Dropwise condensation is a heat transfer enhancement mechanism more commonly observed in vapor space condensation. Heat fluxes and heat transfer coefficients in dropwise condensation on flat plates [1,19–22] or external tubes [23–26] have been found to be 5–20 times higher than filmwise condensation for these external flows. Surface properties such as contact angle [27], surface roughness [20,28,29], and droplet state (i.e., Ref. [30] or [31]) are essential for promoting dropwise condensation. In order to obtain desired surface properties to form dropwise condensation, surfaces have been modified with surface roughness at multiple length scales [20,29,30,32–34], anisotropic patterns [1,28,35], self-assembled monolayers [36,37], electroplating [38], ion implantation [25], and low-surface-energy material coatings [39]. For external flows, droplet nucleation, growth, coalescence, and departure have been identified as critical parameters of heat transfer performance of dropwise condensation [40–45], with decreased thermal resistances for lower droplet sizes [46–48].

In-tube flow condensation differs from vapor space condensation due to higher mass flow rates, and therefore, higher shear stresses at the liquid–vapor interface [49]. Mini- and microchannels offer opportunities for flow condensation enhancement over conventional-sized channels, and few studies have investigated dropwise condensation in mini- and microchannels. Fang et al. [50] obtained 15% heat flux enhancement in a 286 μm diameter hydrophobic silicon channel with a contact angle of 123 deg and a hydrophilic channel with a contact angle of 25 deg. Derby et al. [51] studied steam flow condensation in 1.06 mm mini-gaps of

[1]Corresponding author.

Contributed by the Heat Transfer Division of ASME for publication in the Journal of Heat Transfer. Manuscript received February 18, 2016; final manuscript received April 21, 2016; published online May 17, 2016. Editor: Portonovo S. Ayyaswamy.

hydrophilic copper that measured 1.06 mm with a contact angle of 40 deg and TeflonAF™ coated channels with a contact angle of 120 deg. Condensing steam heat transfer coefficients were found to be 3.2 to 13.4 times that of filmwise condensation. Dropwise condensation and droplet sweeping were hypothesized to be enhancement mechanisms based on heat transfer coefficient measurements.

Flow regimes significantly impact two-phase heat transfer coefficients for internal flows [10,11], and flow regimes have been mapped by Garimella [52] for condensation and Thome et al. [53] for boiling. Kim and Mudawar [54] created a universal condensation heat transfer coefficient predicting model with one correction for annular flow and another correction for slug flow based on a modified Weber number. Visualization and digital image analysis has enabled investigation of flow condensation and underlying flow mechanisms which affect condensation heat transfer. Chen et al. [55] investigated steam condensation in triangular microchannel with hydraulic diameters of 100 μm and 250 μm and observed droplet, annular injection, and slug-bubbly flow. Increased mass flux was shown to enhance condensation heat transfer. Liebenberg et al. [56] observed flow regime transition from annular to intermittent at vapor qualities of 0.48 for smooth-tube and 0.3–0.39 for a microfin tube with a diameter of 17.27 mm at mass fluxes ranging from 300 to 800 kg/m^2 s. Chen and Derby [57] observed cycles of droplet nucleation, growth, and sweeping in a hydrophobic 0.952 mm mini-channel.

The objectives of this study were to combine flow visualization and heat transfer measurements in order to understand flow and heat transfer effects for internal flow condensation. It was hypothesized by Derby et al. [51] that droplet sweeping was responsible for order-of-magnitude condensation heat transfer enhancement in hydrophobic channels; however, flow was not observed in that work to confirm the hypothesis. Research objectives for this work included simultaneous flow visualization and heat transfer measurements in order to understand dropwise condensation in flow condensation, including the effects of droplet nucleation, coalescence and growth, and sweeping. To accomplish this, steam was condensed in hydrophilic and hydrophobic mini-gaps with hydraulic diameters of 0.952 mm for mass fluxes of 50, 75, and 100 kg/m^2 s within a steam quality range of 0.2–0.8; for each case, condensation heat transfer coefficients and videos were recorded and presented.

2 Experimental Apparatus and Methods

2.1 Apparatus. An open-loop steam apparatus was constructed to simultaneously measure condensation heat transfer and capture visual information for a wide range of steam mass fluxes and qualities (Fig. 1). The campus facility provided steam at 550 kPa and then regulated the steam to a pressure of approximately 250 kPa. Three parallel 60 μm pore filters removed small particles, rust, and debris. Since building steam quality was unknown, the steam entered the separation tank to remove excess liquid. A 500 W cartridge heater superheated the steam to 20–30 °C above saturation temperature in order to determine enthalpy with measured temperature and pressure and the precondenser set the test section inlet quality. The precondenser was cooled via a constant temperature bath (Neslab RTE-221) with cooling water flowing rate measured by a Coriolis flow meter (Micro Motion™ F-series sensor and 2700 transmitter). Cooling water inlet and exit temperatures were measured with T-type thermocouple probes, and steam quality exiting the precondenser and entering the test section was found with an energy balance. In the test section, inlet and exit temperatures, inlet pressure, and pressure drop were directly measured. The flow was visualized through a glass window using a Leica Z16 APO macroscope and a FASTEC IL3 high-speed camera (maximum space resolution of 1280 × 1024 at 500 fps and reduced resolution for up to 20,000 fps rate). In the postcondenser, steam fully condensed and passed through a rotameter for visual confirmation of flow stability. The condensate mass flow rate was measured with an electronic scale and timer.

2.2 Test Section. The test section consisted of a cover plate, glass viewing window, interchangeable coupon with mini-gap, oxygen-free copper block for heat flux measurements, a PEEK block with flow inlet and exit, and an aluminum cooling pad (Fig. 2). The mini-gap was milled into an oxygen-free copper coupon with a width of 10 mm, a depth of 0.5 mm, a length of 40 mm, and a hydraulic diameter of 0.952 mm. Leaving the precondenser, steam flowed through the PEEK block and entered and exited the mini-gap at an angle of 20 deg from the horizontal plane. The coupon inlet and exit were sealed to the PEEK block with O-ring seals. Indium thermal interface material connected the coupon to the heat flux measuring block machined out of oxygen-free copper to ensure well-documented thermal conductivity. For temperature gradient measurements, the 20 × 40 × 40 mm copper block had five holes with diameters of 3.5 mm and spaced 8 mm apart vertically. T-type thermocouples with diameters of 3.175 mm were inserted into each hole, and a thermocouple was installed in the coupon 1 mm from the mini-gap in order to determine wall temperature. Heat flux was found using Fourier's law for the heat transfer coefficient and steam quality change in the test section. Thermal paste (Omega Thermo 201) was used to maintain contact between the copper heat flux block and the aluminum cooling pad. Cooling water from the water bath flowed through serpentine channels in cooling pads with a total temperature change of less than 2 °C, ensuring a constant temperature boundary condition. Flow visualization was accomplished from the top with the macroscope (Leica™ Z16 APO) through a tempered glass viewing window that was 3.175 mm thick (Fig. 2). The window was sealed

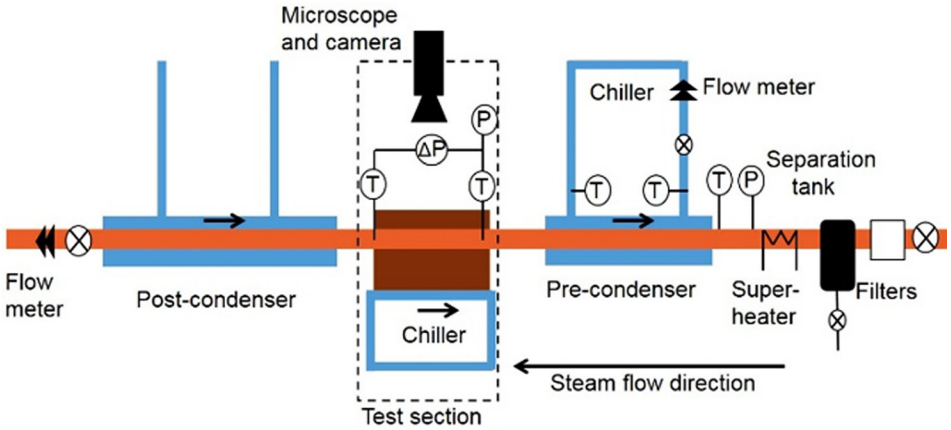

Fig. 1 Flow condensation experimental apparatus

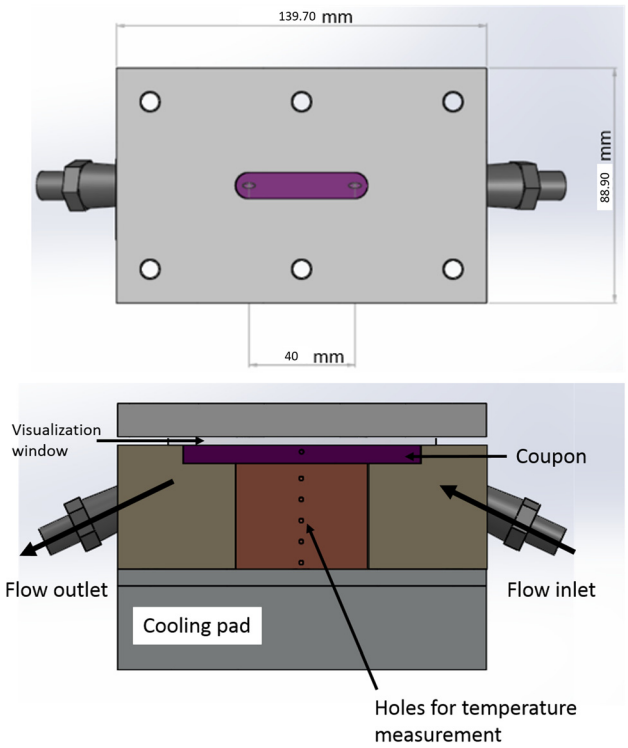

Fig. 2 Front (left) and top (right) views of test section

to the coupon via an O-ring seal, and a cover plate on the top glass window provided pressure for sealing. The entire test section was clamped with five bolts from the cover plate to the cooling pads; bolts were torqued in a diamond pattern for optimal interface heat conduction and O-ring sealing.

2.3 Surface Preparation. Flow condensation experiments were conducted on a bare copper hydrophilic coupon and a Teflon AF™-coated hydrophobic coupon. A goniometer measured the contact angle of a water droplet on the hydrophilic surface to be 70 ± 3 deg (Fig. 3). The hydrophobic mini-gap was dip-coated [51]. The coupon was initially put into a UV machine (ProCleaner™ 110) for 30 min and then soaked in isopropanol for 10 min to remove small particles and the oxide layer. The coupon was then dipped twice in a solution of DuPont Teflon AF™ Grade 400s2-100-1 and FC-40 solvent. Subsequently, the coupon was baked at 105 °C for 1 hr to remove the solvent and then 165 °C for 24 hrs to create a uniform coating. After the dip-coating process, the contact angle was measured to be 110 ± 3 deg (Fig. 3).

2.4 Single-Phase Validation Data Reduction. The goals of single-phase validation tests were to verify the accuracy of heat transfer measurements and to quantify heat loss from the glass window. In the single-phase validation tests, steam was fully condensed in the precondenser and cooled in the test section. An energy balance was conducted on the condensate via Fourier's law. The cooling rate of the condensate was obtained using the following expression:

$$\dot{Q}_{st} = \dot{m}_{st} c_p (T_{in} - T_{out}) \tag{1}$$

where $\dot{Q}_{st}$ was the condensate heat transfer rate, $\dot{m}_{st}$ was the hot-side mass flow rate, c_p was the specific heat of water, and T_{in} and T_{out} were the inlet and exit temperatures, respectively. Fourier's law was applied to the copper block

$$\dot{Q}_{bl} = -k_{cu} W_{bl} L_{bl} \frac{dT}{dy} \tag{2}$$

where $\dot{Q}_{bl}$ was the heat transfer rate measured in the copper block, k_{cu} was the conductivity of oxygen-free copper, W_{bl} and L_{bl} were the width and length of the copper block, and dT/dy was the temperature gradient. The temperature gradient was the slope obtained from a linear regression of five temperature measurements in the block. Additionally, single-phase Nusselt numbers were obtained using the heat transfer rate measured in the copper block.

Heat loss through the glass window in the test section is the difference between the heat transfer rates measured with and without the insulation cover on the top of the glass window. It was quantified with the following equation:

$$\dot{Q}_{loss} = \dot{Q}_{w,ins} - \dot{Q}_{wo,ins} \tag{3}$$

where $\dot{Q}_{loss}$ was the heat loss from the glass window, $\dot{Q}_{wo,ins}$ was the measured heat transfer rate in the block with thermal insulation on the top of glass window, and $\dot{Q}_{wo,ins}$ was the measured heat transfer rate in the block without the thermal insulation on the top of glass window.

2.5 Condensation Heat Transfer Coefficient Data Reduction. Condensation heat transfer coefficients were calculated using Newton's law of cooling

$$h = \frac{q''_{cond}}{T_{st} - T_s} = \frac{\dot{Q}_{bl} \dfrac{W_{bl} L_{bl}}{A_{cond}}}{T_{st} - T_s} \tag{4}$$

where h was the heat transfer coefficient, q''_{cond} was the heat flux normal to the condensation surface, A_{cond} was the condensation area of the mini-gap, T_{st} and T_s were the steam temperature and surface temperatures at the center point of the mini-gap, respectively, and W_{bl} and L_{bl} were the width and length of the mini-gap, respectively. The surface temperature was obtained via direct

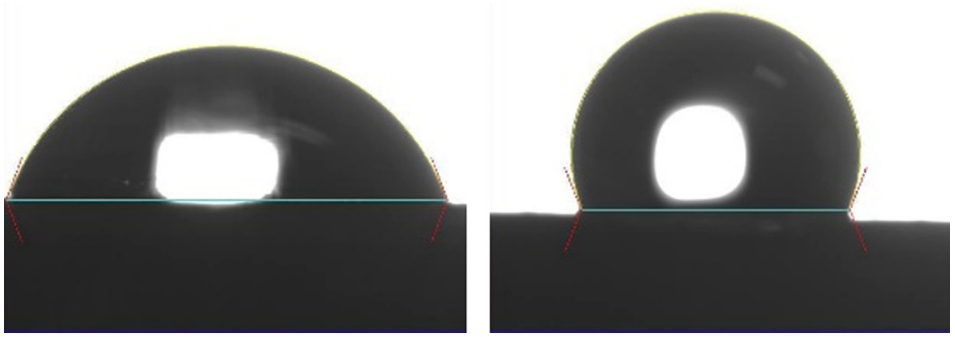

Fig. 3 Contact angle of water on bare copper surface (left) and Teflon AF™-treated hydrophobic surface (right)

thermocouple measurement 1 mm below the condensation surface. Fluid temperature at the center point was found with local pressure P_{st}, calculated with following equation:

$$P_{st} = P_{in} - \Delta P = P_{in} - \Delta P_{inlet} - \frac{1}{2}\Delta P_{gap} \tag{5}$$

where P_{st} was the steam pressure at the center point, P_{in} was the inlet pressure, ΔP was the pressure drop from the inlet to the center point, ΔP_{inlet} was the pressure drop in the inlet tube, and ΔP_{gap} was the pressure drop in the mini-gap. The pressure drop model in the test section consisted of three segments: an inlet tube with a diameter of 2 mm, a condensation mini-gap, and an outlet tube with a diameter of 2 mm. This pressure drop model was compared to the experimental pressure drop obtained with a differential pressure transducer (Omega PX409); agreement was excellent (Fig. 4), resulting in uncertainties in fluid temperature of ±0.2 °C. Pressure drops in the test section were predicted with the two-phase pressure drop model by Lockhart and Martinelli [58], which was modified by Kim and Mudawar [59] for condensation in mini- and microgaps

$$\left(-\frac{\Delta P}{\Delta z}\right)_{TP} = \phi_f^2\left(-\frac{\Delta P}{\Delta z}\right)_f = \left(1 + \frac{C}{\chi} + \frac{1}{\chi^2}\right)\left(-\frac{\Delta P}{\Delta z}\right)_f \tag{6}$$

$$\chi^2 = \frac{\left(\frac{\Delta P}{\Delta z}\right)_f}{\left(\frac{\Delta P}{\Delta z}\right)_g} \tag{7}$$

$$\Delta P_{pred} = \Delta P_{inlet} + \Delta P_{gap} + \Delta P_{outlet} \tag{8}$$

where $\Delta P/\Delta z$ was the pressure gradient, ϕ_f was the two-phase multiplier, χ was Lockhart–Martinelli parameter, $(\Delta P/\Delta z)_f$ and $(\Delta P/\Delta z)_g$ were the frictional pressure gradient with liquid or gas only, respectively, and ΔP_{pred}, ΔP_{inlet}, ΔP_{gap}, and ΔP_{outlet} were predicted pressure drops in the entire test section, inlet tube, condensation mini-gap, and outlet tube, respectively.

2.6 Uncertainty Analysis. Care was taken to ensure accurate measurements. T-type thermocouples were calibrated in a water bath at seven temperature points, plus ice and boiling points, against a thermometer (Omega HH41) with an accuracy of ±0.05 °C in order to obtain a resultant temperature measurement uncertainty of ±0.2 °C. The uncertainty of temperature gradient in the copper block was calculated using an equation developed by Kedzierski and Worthington [60]

$$w_g = \sqrt{w_{Ti}^2 + \left(\frac{q''D}{6k_{cu}}\right)^2}\sqrt{\frac{1}{\sum_{i=1}^{N}(y_i - \bar{y})^2}} \tag{9}$$

where w_{Ti} was the calibrated thermocouple uncertainty, y_i was the distance of the ith thermocouple from the condensation surface, and $\bar{y}$ was the average distance of the thermocouple from the condensation surface. Due to the high conductivity of oxygen-free copper, large spacing between holes, and the small diameter of the holes, the gradient uncertainty was a maximum of ±2%. Pressure transducers were calibrated with a deadweight tester to obtain full range uncertainty of 0.25% (1.7 kPa). Condensate mass flow rates were measured with an electronic scale, and flow stability was visually monitored with a rotameter at the end of the steam line. Mass flow rate uncertainties contributed minimally to the system uncertainties because each test lasted more than 10 min and the flow was very stable (mass flow rate fluctuated less than ±2%). In general, uncertainties in quality were ±0.01–0.02. The precondenser and test section were insulated with fiberglass to prevent ambient heat loss, and the glass window in the test section was insulated during heat transfer data acquisition; the insulation was removed for taking video.

Propagation of uncertainty analysis was conducted using the approach by Kline and McClintock [61]

$$w_h^2 = \left(\frac{\omega_{q'',cond}}{T_{st} - T_s}\right)^2 + \left(\frac{\omega_{T_{st}}}{(T_{st} - T_s)^2}\right)^2 + \left(\frac{\omega_{T_s}}{(T_{st} - T_s)^2}\right)^2 \tag{10}$$

where w_h was the propagated uncertainty for the heat transfer coefficient, $\omega_{q'',cond}$ was the propagated uncertainty of heat flux in the mini-gap, and $\omega_{T_{st}}$ and ω_{T_s} were steam temperature and surface temperature uncertainties, respectively. Heat transfer coefficient uncertainties are reported in Secs. 3.2 and 3.3.

In addition, the uncertainty in test section steam quality was estimated through a propagation of uncertainty approach. The primary contributor to uncertainty in quality was from the precondenser, which is a tube-in-tube heat exchanger. Cooling water entered the precondenser at a temperature of 20 to 35 °C, and an energy balance was conducted on the coolant. For test purposes, the coolant energy balance was compared to the energy change of fully condensing superheated vapor into single-phase liquid. The cooling side heat transfer rate matches the steam side heat transfer rate within ±4%, indicating negligible heat loss.

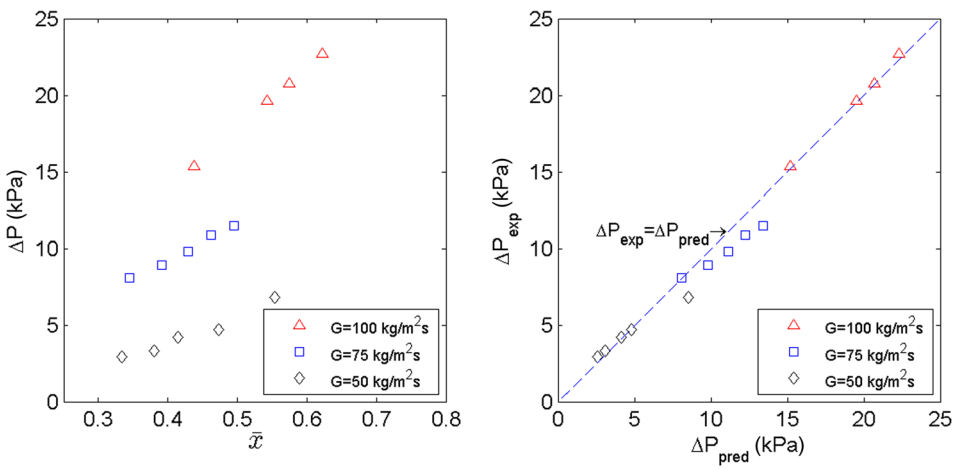

Fig. 4 Experimental pressure drop (left) and comparison of experimental results and pressure drop model (right)

Average test section quality was calculated from inlet quality, x_{in}, and change in quality across the test section, Δx

$$\bar{x} = x_{in} - \frac{1}{2}\Delta x \tag{11}$$

where the inlet quality was determined through an energy balance on the precondenser

$$x_{in} = \frac{h_{in} - h_{sat,f}}{h_{fg}} = \frac{h_{shv} - \dfrac{\dot{Q}_{PC}}{\dot{m}_{st}} - h_{sat,f}}{h_{fg}} = \frac{h_{shv} - \dfrac{\dot{m}_{cooling}\ Cp\ \Delta T}{\dot{m}_{st}} - h_{sat,f}}{h_{fg}} \tag{12}$$

and the change in test section quality was determined through the test section energy balance

$$\Delta x = \frac{\dot{Q}_{bl}}{\dot{m}_{st} h_{fg}} = \frac{-k\dfrac{dT}{dy}A_{bl}}{\dot{m}_{st} h_{fg}} \tag{13}$$

Resulting uncertainties in average test section quality were calculated

$$\omega^2(\bar{x}) = \left(\frac{\dot{m}_{cooling}\ Cp}{\dot{m}_{st}\ h_{fg}}\right)^2 \omega(\Delta T)^2 + \left(\frac{1}{\dot{m}_{st} h_{fg}}\right)^2 \omega(\dot{Q}_{bl})^2 \tag{14}$$

The contribution of uncertainty from the cooling water flow rate was very small due to the accuracy of the Coriolis flow meter, and the uncertainty of the steam flow rate was negligible due to the stable flow rate and long time duration. The resultant maximum value in steam quality uncertainty was ± 0.02, and therefore is not shown in the figures.

3 Results and Discussion

3.1 Single-Phase Validation. Single-phase tests validated the heat transfer rate measurement in the cooper block, heat loss from the glass window, and heat transfer coefficient measurement. In the tests, the test section heat transfer rate ranged from 40 to 80 W (Fig. 5(*a*)) corresponding to inlet temperature ranging from 75 to 110 °C. Cooling side temperature was maintained constant (35 °C). and therefore, higher inlet temperature corresponds to higher heat flux and larger temperature drop in the test section. The single-phase energy balance was compared to the heat flux obtained via Fourier's law. The agreement was very good at most heat fluxes (Fig. 5(*a*)), but was reduced when single-phase condensate temperature changes approached 40 °C at the highest heat transfer rate. At a fluid temperature change of 40 °C, it is likely that heat losses and axial conduction affected heat transfer measurement; however, this large temperature drop was not encountered in two-phase testing since condensing steam temperature changes were less than 5 °C. Heat loss through glass window was calculated by comparing the heat transfer rate in the copper block with and without an insulation cover, measured at various water temperatures (70–110 °C), and heat losses were always less than 5% (Fig. 5(*b*)). In the two-phase tests, steam-condensing temperatures ranged from 120 to 130 °C. Heat losses through the visualization window decreased steam quality by less than 0.001 and were considered negligible. For further validation of the test section, single-phase Nusselt numbers were measured for laminar flows (Fig. 6). Due to the high aspect ratio of the channel (20:1), the experimental data were compared against the theoretical case for flat plates with one plate insulated (Nu = 4.86) and the resulting agreement was very good.

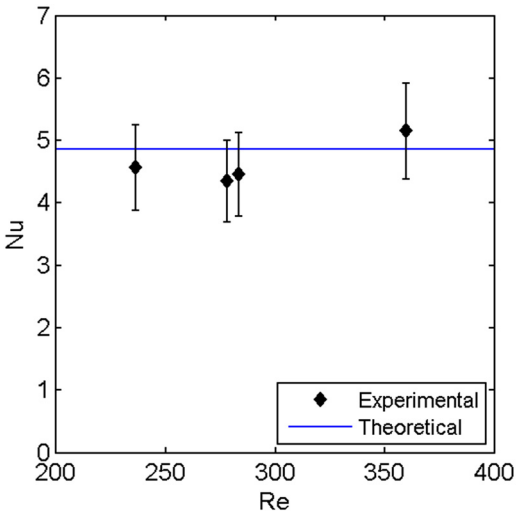

Fig. 6 Single-phase heat transfer measurement validation tests comparing experimental results to convection in two infinite plates with one side insulated

3.2 Condensation Heat Transfer and Flow Visualization in a Hydrophilic Mini-Gap. After the experimental apparatus was validated, condensation heat transfer and flow visualization

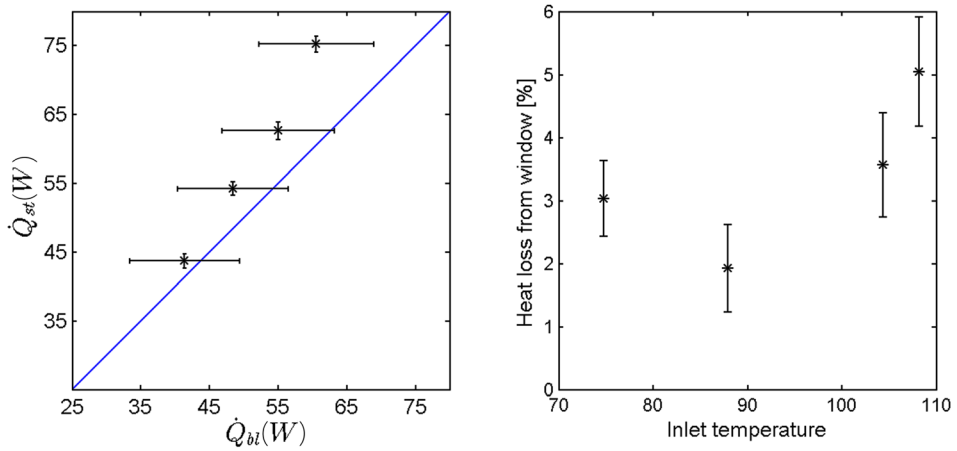

Fig. 5 Single-phase validation tests: (*a*) heat transfer rates, and (*b*) heat loss through the visualization window

experiments were conducted in the bare copper hydrophilic mini-gap at mass fluxes of 50, 75, and 100 kg/m^2 s for a range of qualities. In general, quality changes were low ($\leq$0.2) through the mini-gap, although quality changes increased slightly at the lowest mass flux of 50 kg/m^2 s. For all cases, filmwise condensation was observed in the hydrophilic mini-gap (Fig. 10(*a*)). Pressure drop and heat transfer coefficients in the hydrophilic mini-gap at mass fluxes of 50, 75, and 100 kg/m^2 s for qualities are reported in Figs. 4 and 7. Pressure drop increased with increased steam qualities or mass fluxes, corresponding to increased superficial or average velocity. The heat transfer coefficient increased with increased steam qualities and mass fluxes, corresponding to decreased condensate film layer thickness.

For tests in the hydrophilic mini-gap, condensation heat transfer data were compared to the Kim and Mudawar [54] correlation for filmwise condensation in micro- and mini-channels. The correlation was developed for a number of fluids, primarily refrigerants, for diameters ranging from 0.424 to 6.22 mm. The correlation was assessed using MAE, defined as

$$\text{MAE} = \frac{1}{n}\sum_{i=1}^{n}\left|\frac{h_{\text{pred}} - h_{\text{exp}}}{h_{\text{exp}}}\right| \tag{15}$$

where h_{pred} was the heat transfer coefficient obtained from the Kim and Mudawar [54] correlation, h_{exp} was the experimentally measured heat transfer coefficient, and n was the total number of data. The MAE of experimental results from the Kim and Mudawar model [54] was 20.19% (Fig. 8), demonstrating good prediction of the experimental data for the hydrophilic mini-gap. The experimental results were higher than the model, particularly at lower qualities, with several possible contributing factors. First, the correlation was developed primarily for refrigerants, but water has a higher surface tension value. Surface tension may cause condensate to gather in sharp mini-channel corners, thereby thinning the liquid film around the perimeter and increasing heat transfer, although this liquid film thinning is dependent on the fluid and geometry [62–65]. Second, the mini-gap had a large aspect ratio (20:1), and the flow was developing in the test section. Overall, the Kim and Mudawar [54] correlation accurately predicted the data for the hydrophilic mini-gap.

3.3 Condensation Heat Transfer and Flow Visualization in a Hydrophobic Mini-Gap. Flow condensation was studied in a hydrophobic mini-gap for three mass fluxes and a range of qualities. Dropwise condensation was observed in the hydrophobic mini-gap, and correspondingly higher heat transfer coefficients were recorded compared to the hydrophilic surface. The results are discussed in Secs. 3.3.1–3.3.4.

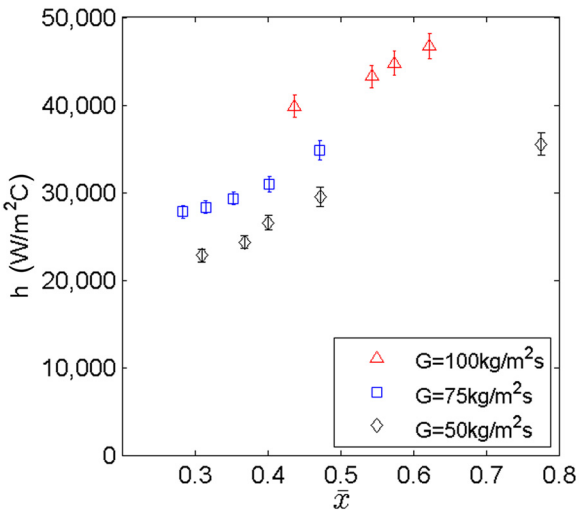

Fig. 7 Condensation heat transfer coefficients in hydrophilic gap

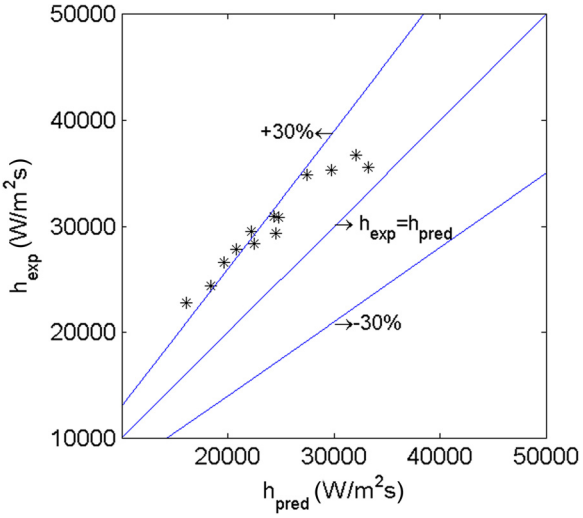

Fig. 8 Experimentally measured filmwise condensation and heat transfer coefficients predicted by Kim and Mudawar [54] in the hydrophilic mini-gap

3.3.1 Visualization of Dropwise Condensation. Condensation was studied in a hydrophobic mini-gap at mass fluxes of 50–100 kg/m^2 s. Periodic droplet nucleation, coalescence, and departure stages were observed in hydrophobic mini-gaps; no droplets were observed in the hydrophilic mini-gap (Figs. 9 and 10). Depending on the mass flux and quality, water in the hydrophobic mini-gap could completely cover the surface with small droplets or form larger droplets or rivulets. Droplet size is an important parameter that governs condensation since small droplets account for the largest portion of heat transfer [46,66,67], and departure droplet size was observed to be a function of mass flux and quality. The largest droplets were observed for the lowest flow rate of 50 kg/m^2 s, and droplet size decreased as mass flux and shear forces increased (Fig. 10).

3.3.2 Sweeping Appearance and Heat Transfer With Various Mass Fluxes. Videos were analyzed at the center point for conditions of identical average quality ($\bar{x} = 0.42$) and differing mass fluxes of 50, 75, and 100 kg/m^2 s. Videos were taken at 250 fps and were reviewed frame by frame with ImageJ™ and PFV™ (PHOTRON FASTCAM VIEWER) software. The cycle began with

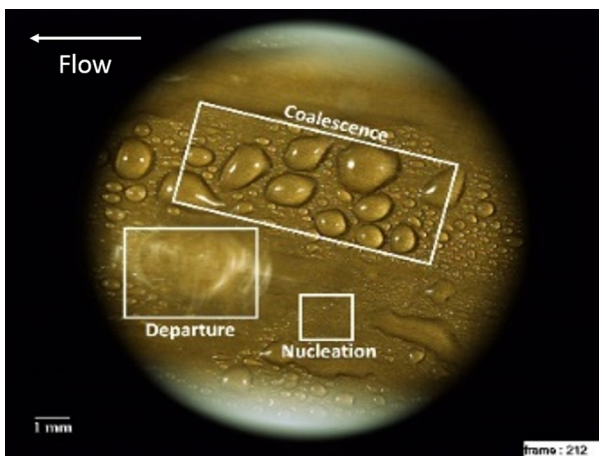

Fig. 9 Nucleation, coalescence, and departure states of droplets in a hydrophobic mini-gap

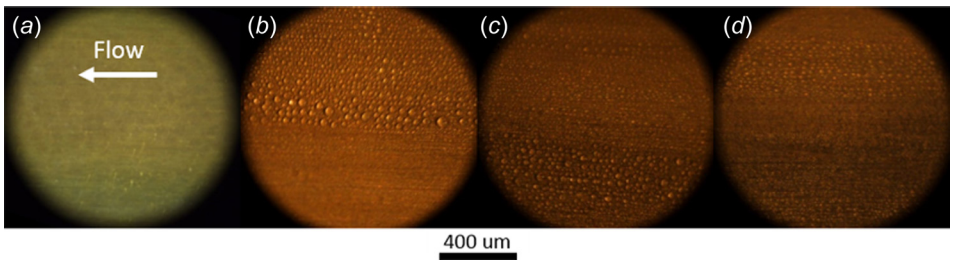

Fig. 10 Condensation modes in (*a*) hydrophilic $G = 50\,kg/m^2\,s$ and hydrophobic surface, (*b*) $G = 50\,kg/m^2\,s$, (*c*) $G = 75\,kg/m^2\,s$, and (*d*) $G = 100\,kg/m^2\,s$

nucleation, followed by coalescence, and ended at the frame at which the droplets departed. Three typical sweeping periods of three mass fluxes are depicted in Fig. 11.

Sweeping cycle periodicity allowed for the identification of the sweeping frequency. Videos were taken for conditions of identical steam quality of 0.42 and mass fluxes of 50, 75, and 100 kg/m^2 s. A 1 mm × 1 mm area was selected near the center point to determine the sweeping periods. Cycles beginning with nucleation and ending with a majority of droplets with uniform dimensions in the view were swept. Twenty cycles were identified for each scenario. At the lowest mass flux of 50 kg/m^2 s, the widest range in sweeping periods were observed, 12 to 77 ms, with an average value of 28 ms and standard deviation of 15 ms. For $G = 75\,kg/m^2$ s, the sweeping period range was smaller, 12 to 32 ms, with an average value of 23 ms and standard deviation of 6 ms. For the highest mass flux $G = 100\,kg/m^2$ s, the sweeping period range was the narrowest, 7.2 to 24 ms, with an average value of 17 ms and standard deviation of 4.4 ms (Figs. 11 and 12). Droplet departure diameters were measured for each mass flux for a cycle with a sweeping period close to the average value for that mass flux. Since the effects of shear are of primary interest, reported droplet diameters include only droplets moved via interfacial shear forces. Analyzing the same area where sweeping periods were found, the average departure diameter were $13.7 \pm 4.5\,\mu m$, $12.9 \pm 4.0\,\mu m$,

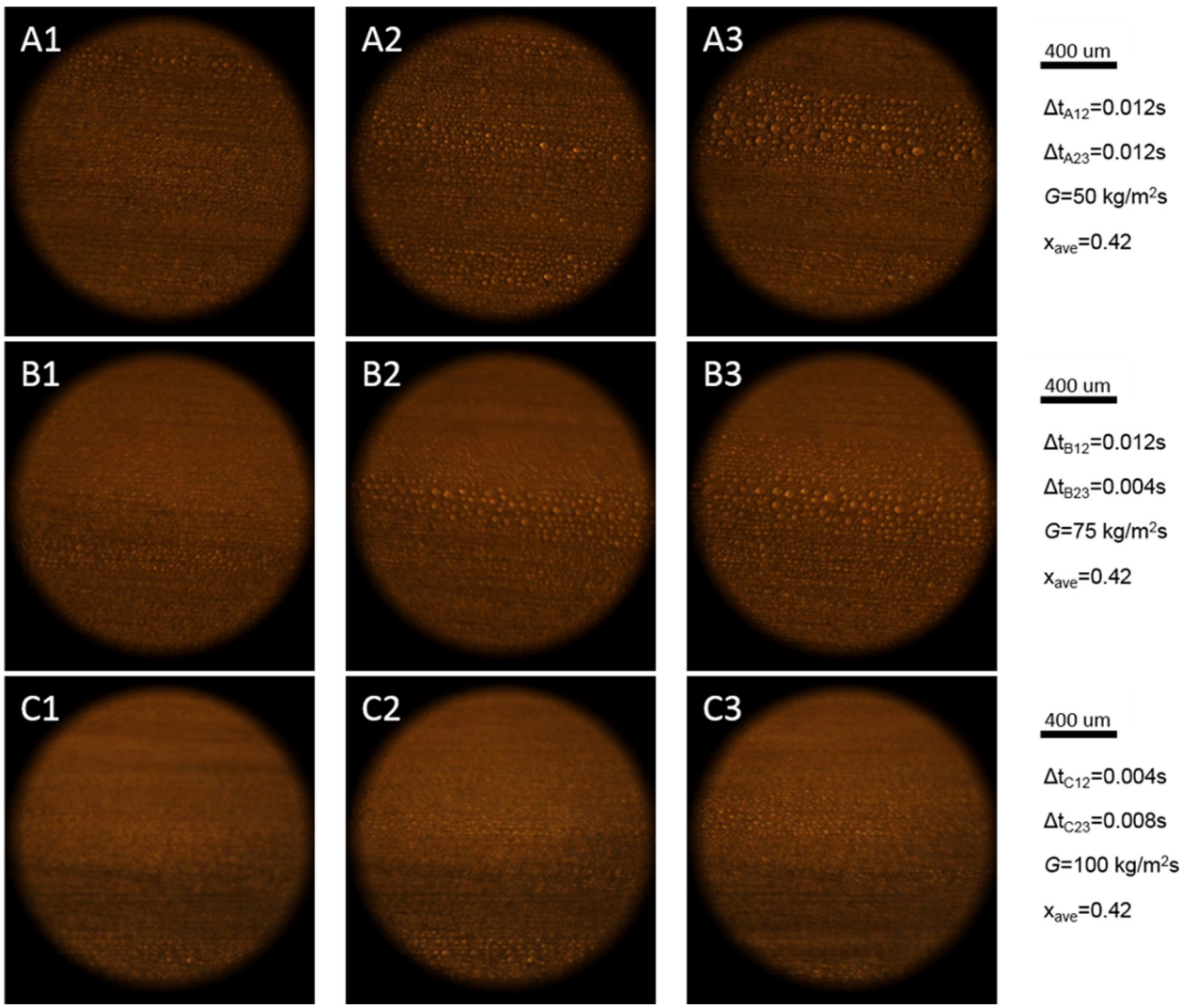

Fig. 11 Nucleation, coalescence, and departure stages with steam quality of 0.42 and mass fluxes of 50, 75, and 100 kg/m^2 s

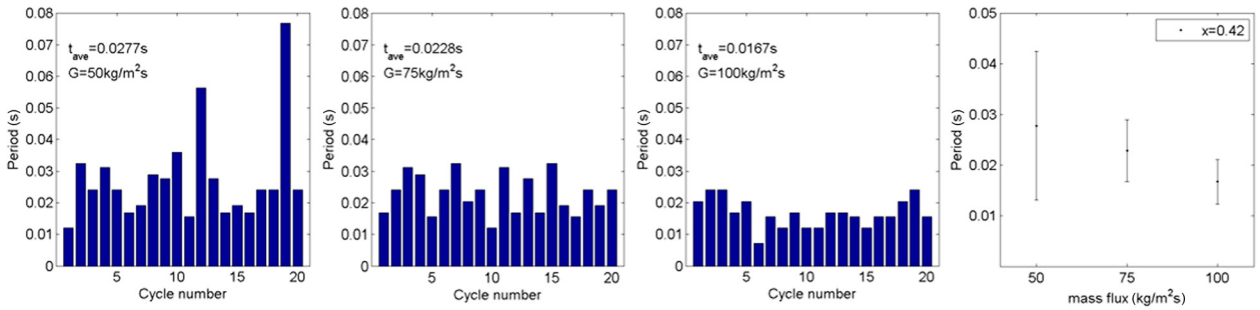

Fig. 12 Comparison of sweeping periods at average steam quality of 0.42 at mass fluxes of (*a*) 50, (*b*) 75, (*c*) 100 kg/m^2 s, and (*d*) sweeping periods with standard deviations

Table 1 Droplet departure diameter at different mass fluxes and qualities

Mark	Mass flux (kg/m^2 s)	Steam quality	Average departure diameter (μm)	Standard deviation (μm)	Largest departure diameter (μm)
A	50	0.42	13.7	4.5	26.40
B	75	0.42	12.9	4.0	21.19
C	100	0.42	10.3	1.0	11.99
D	50	0.35	32.0	16	64.36
E	50	0.42	13.7	4.5	26.40
F	50	0.55	10.6	1.5	13.92

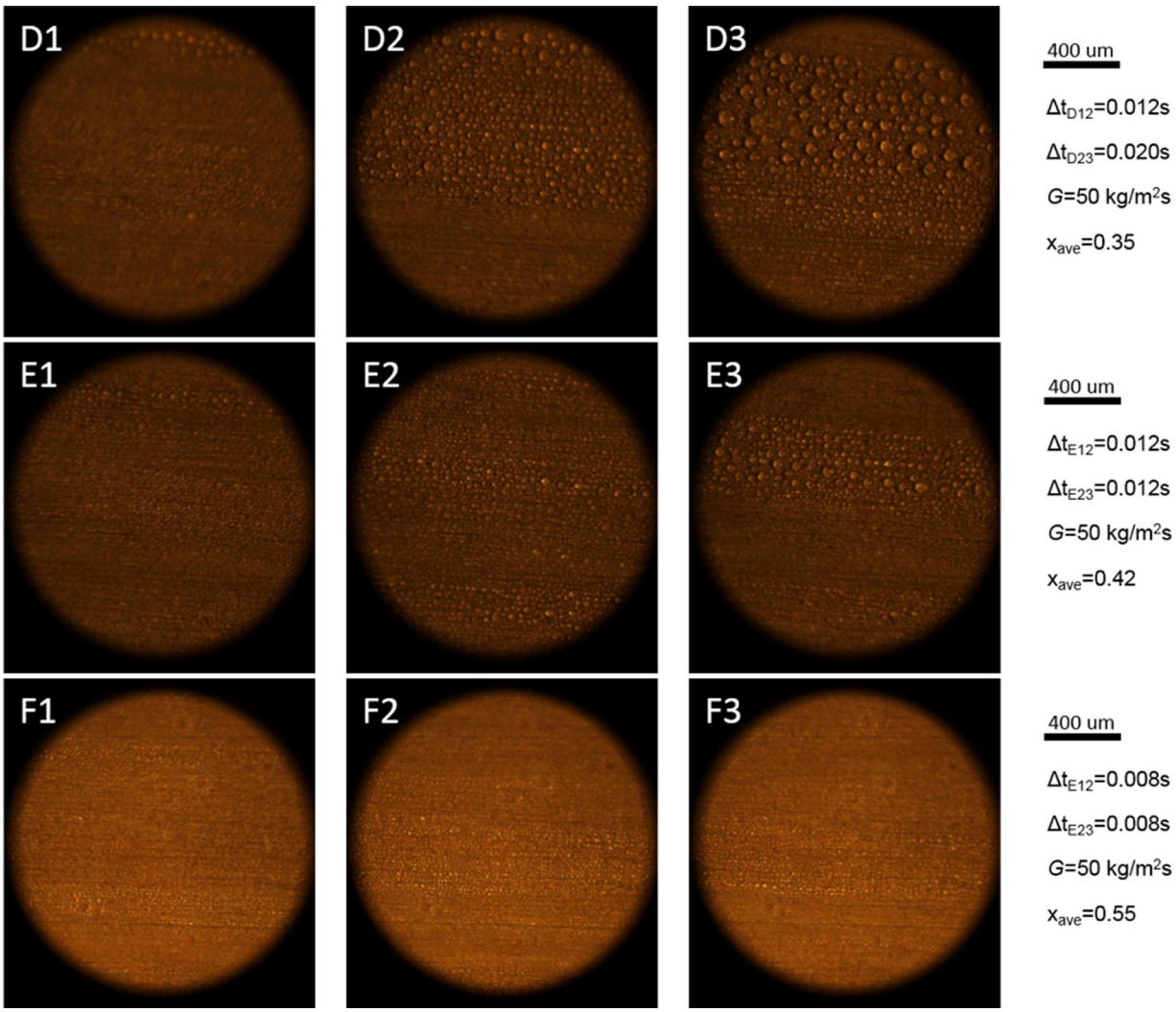

Fig. 13 Nucleation, coalescence, and departure stages with $G = 50$ kg/m^2 s and steam qualities of 0.35, 0.42, and 0.55

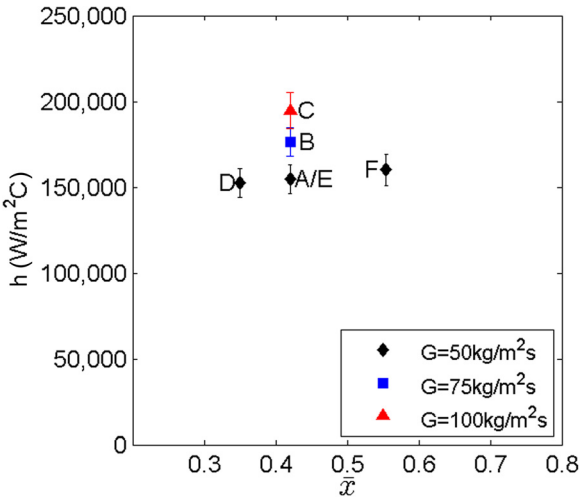

Fig. 14 Heat transfer coefficient on hydrophobic surface corresponding to conditions in Figs. 11 and 13

and $10.3 \pm 1.0\,\mu$m for mass fluxes of 50, 75, and 100 kg/m^2 s, respectively, (Table 1). At the same quality, droplet departure diameter sizes decreased with increasing mass flux.

Heat transfer coefficients were measured for the cases depicted in Figs. 11 and 13. Decreased droplet size and increased droplet sweeping frequency reduced thermal resistance between steam and solid, thereby increasing the heat transfer coefficients. Heat transfer coefficients were given for cases corresponding to A–F (Fig. 14). At an average steam quality of 0.42, condensation heat transfer coefficients increased from 154,700 to 176,500 to 194,800 at steam mass fluxes of 50, 75, and 100 kg/m^2 s, respectively. With mass flux of 50 kg/m^2 s, only modest increases in the heat transfer coefficient were observed at qualities of 0.35–0.55 (Fig. 14). The largest droplets ($32 \pm 16\,\mu$m) were observed at the lowest mass flux of 50 kg/m^2 s and quality of 0.35 (Fig. 14), and exhibited the lowest heat transfer coefficients measured in the hydrophobic channel (Table 1).

3.3.3 Sweeping Appearance and Heat Transfer With Various Qualities. Additional visualization studies were conducted to understand the impact of quality on a fixed mass flux. Periodiclike cycles of nucleation, coalescence, and departure were found. At a mass flux maintained at 50 kg/m^2 s, typical cycle periods in Fig. 13 were 32 ms, 24 ms, and 16 ms with steam qualities of 0.35, 0.42, and 0.55, respectively. Droplet departure diameters were analyzed for average cycles. Analyzing the same area where sweeping periods were found, the average departure diameter were, respectively, $32 \pm 16\,\mu$m, $13.7 \pm 4.5\,\mu$m, and $10.6 \pm 1.5\,\mu$m for qualities of 0.35, 0.42, and $x = 0.55$, respectively, (Table 1).

3.3.4 Condensation Heat Transfer Coefficients in the Hydrophobic Mini-Gap. Dropwise condensation was observed in the hydrophobic mini-gap increasing condensation heat transfer coefficients compared to filmwise condensation in the hydrophilic mini-gap. Condensation heat transfer coefficients are presented in Fig. 15. Uncertainties in the condensation heat transfer coefficient were $\pm 4.5\%$ to $\pm 10.1\%$, substantially reduced compared to over $\pm 40\%$ in the work of Derby et al. [51] due to low fluid-wall temperature differences. Uncertainty reductions were obtained due to a taller test section and higher measured fluid-wall temperature differences, approximately 3–7 °C. In the range measured, increases in quality only had modest effects on the heat transfer coefficient, while increases in mass flux increased heat transfer coefficients. Based on flow visualization, droplet departure diameters were smaller for high mass fluxes at the same quality. The hypothesis was made that this reduction in droplet departure size, and therefore, liquid film resistance was responsible for the increase in heat transfer coefficients with respect to mass flux.

Flow condensation heat transfer coefficients in the hydrophobic gap were compared to the measured filmwise condensation heat transfer coefficients in the hydrophilic gap (Fig. 16). Heat transfer coefficient enhancement is defined as

$$\epsilon = \frac{h_{\text{phobic}}}{h_{\text{philic}}} \tag{16}$$

where ϵ was the ratio of experimental data over predicted data, h_{phobic} was the experimentally measured heat transfer coefficient in the hydrophobic gap, and h_{pre} was the corresponding heat transfer coefficient in a hydrophilic gap for a specific mass flux, G, and steam quality, x. Experimental data with hydrophobic mini-gap showed 480–614% enhancement over the hydrophilic mini-gap. Highest enhancements were observed at the lowest qualities, in which the liquid film created the highest filmwise resistance.

4 Conclusions

Condensation experiments were conducted in hydrophilic and hydrophobic 0.952 mm diameter mini-gaps; flow visualization and heat transfer data were simultaneously recorded. Filmwise condensation was observed in the hydrophilic (contact angle 70 deg) mini-gap, whereas dropwise condensation were observed on the Teflon AF™-coated hydrophobic surface (contact angle 110 deg). The following observations were made and conclusions were drawn:

(a) Periodic cycles of droplet nucleation, coalescence, and departure were observed in dropwise condensation in the hydrophobic mini-gap.

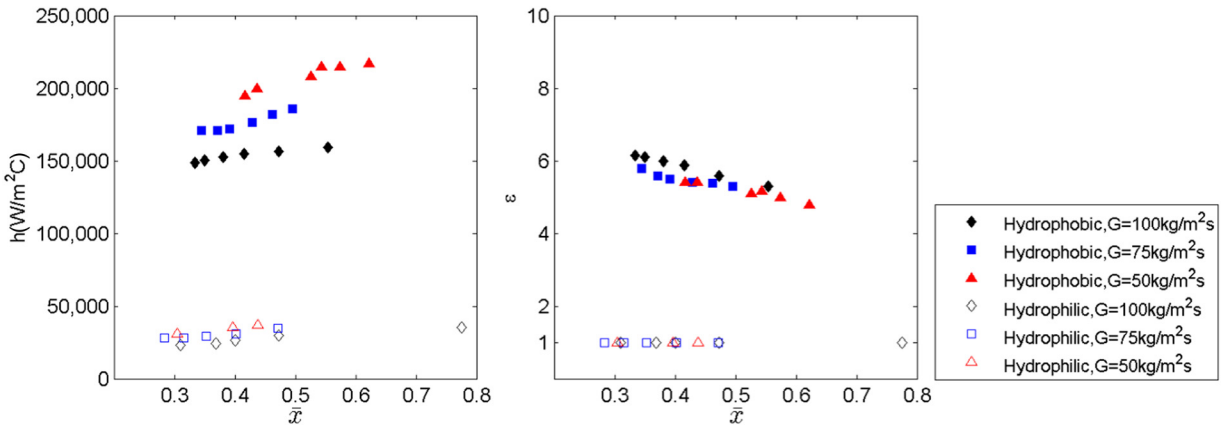

Fig. 15 Heat transfer coefficient enhancement of hydrophobic mini-gap

(b) When the average steam quality was fixed ($\bar{x} = 0.42$), the average sweeping period decreased from 28 to 23 to 17 ms for mass fluxes of 50, 75, and 100 kg/m^2 s, respectively, and the average droplet departure diameters decreased from 13.7 to 12.9 to 10.3 μm.
(c) When the steam mass flux was fixed ($G = 50$ kg/m^2 s), the average sweeping periods of 32, 24, and 16 ms and average departure diameters of 32, 13.7, and 10.6 μm were found at average steam qualities of 0.35, 0.42, and 0.55, respectively.
(d) Reduced droplet departure size and sweeping periods corresponded to increased condensation heat transfer coefficients, demonstrating the importance of droplet sweeping for reducing condensate liquid resistances, and enhancing flow condensation.

Acknowledgment

The authors would like to thank the Kansas State University Electric Power Affiliates Program for providing partial support of this project, and Eric Kerschen and Kevin Bultongez for their assistance constructing the experimental apparatus.

Nomenclature

A = area, m^2
Cp = specific heat, kJ/(kg K)
D = diameter, m
G = mass flux, kg/(m^2 s)
h = heat transfer coefficient, W/(m^2 K)
k = thermal conductivity, W/(m K)
L = length, m
$\dot{m}$ = mass flow rate, kg/s
P = pressure, kPa
$\dot{Q}$ = heat transfer rate, W
q'' = heat flux, W/m^2
R = thermal resistance, m^2 k/W
t = sweeping period, s
T = temperature, °C
W = width, m
y = vertical location, m
Z = characteristic length, m

Greek Symbols

ϵ = heat transfer coefficient enhancement
Φ = two-phase pressure drop multiplier
χ = Lockhart–Martinelli parameter
ω = uncertainty

Subscripts

bl = block
cond = condensation
cooling = cooling water
cu = copper
exp = experimental result
f = fluid
g = temperature gradient
gap = condensation mini-gap
in = test section inlet
inlet = inlet tube test section
out = test section outlet
philic = hydrophilic
phobic = hydrophobic
pred = predicted result
s = surface
st = steam
TP = two phase
w, ins = with insulation
wo, ins = without insulation

References

[1] Baojin, Q., Li, Z., Hong, X., and Yan, S., 2011, "Experimental Study on Condensation Heat Transfer of Steam on Vertical Titanium Plates With Different Surface Energies," Exp. Therm. Fluid Sci., **35**(1), pp. 211–218.
[2] USEIA, 2014, "Annual Energy Outlook 2014 with projections to 2040," U.S. Energy Information Administration, Washington, DC, Paper No. DOE/EIA-0383.
[3] Tidwell, V. C., Macknick, J., Zemlick, K., Sanchez, J., and Woldeyesus, T., 2014, "Transitioning to Zero Freshwater Withdrawal in the U.S. for Thermoelectric Generation," Appl. Energy, **131**, pp. 508–516.
[4] Shin, J. S., and Kim, M. H., 2005, "An Experimental Study of Flow Condensation Heat Transfer Inside Circular and Rectangular Mini-Channels," Heat Transfer Eng., **26**(3), pp. 36–44.
[5] Agarwal, A., and Garimella, S., 2010, "Representative Results for Condensation Measurements at Hydraulic Diameters ~100 Microns," ASME J. Heat Transfer, **132**(4), p. 041010.
[6] Fang, C., David, M., Rogacs, A., and Goodson, K., 2010, "Volume of Fluid Simulation of Boiling Two-Phase Flow in a Vapor-Venting Microchannel," Front. Heat Mass Transfer, **1**(1), p. 013002.
[7] Bandhauer, T. M., Agarwal, A., and Garimella, S., 2006, "Measurement and Modeling of Condensation Heat Transfer Coefficients in Circular Microchannels," ASME J. Heat Transfer, **128**(10), pp. 1050–1059.
[8] Webb, R. L., and Ermis, K., 2001, "Effect of Hydraulic Diameter on Condensation of R-134A in Flat, Extruded Aluminum Tubes," J. Enhanced Heat Transfer, **8**(2), pp. 77–90.
[9] Kandlikar, S. G., 2001, "Fundamental Issues Related to Flow Boiling in Minichannels and Microchannels," Exp. Therm. Fluid Sci., **26**(2–4), pp. 389–407.
[10] Chen, Y., Shi, M., Cheng, P., and Peterson, G., 2008, "Condensation in Microchannels," Nanoscale Microscale Thermophys. Eng., **12**(2), pp. 117–143.
[11] Cheng, P., Wang, G., and Quan, X., 2009, "Recent Work on Boiling and Condensation in Microchannels," ASME J. Heat Transfer, **131**(4), p. 043211.
[12] Wang, W.-W. W., Radcliff, T. D., and Christensen, R. N., 2002, "A Condensation Heat Transfer Correlation for Millimeter-Scale Tubing With Flow Regime Transition," Exp. Therm. Fluid Sci., **26**(5), pp. 473–485.
[13] Coleman, J. W., and Garimella, S., 2003, "Two-Phase Flow Regimes in Round, Square, and Rectangular Tubes During Condensation of Refrigerant R134a," Int. J. Refrig., **26**(1), pp. 117–128.
[14] Garimella, S., 2004, "Condensation Flow Mechanisms in Microchannels: Basis for Pressure Drop and Heat Transfer Models," Heat Transfer Eng., **25**(3), pp. 104–116.
[15] Cavallini, A., Censi, G., and Del Col, D., 2003, "Condensation à l'extérieur et à l'intérieur de Tubes lisses et à Surface augmentée—Point sur le recherche récente," Int. J. Refrig., **26**(4), pp. 373–392.
[16] Chowdhury, S., Al-Hajri, E., Dessiatoun, S., Shooshtari, A., and Ohadi, M., 2006, "A Experimental Study of Condensation Heat Transfer and Pressure Drop in a Single High Aspect Ratio Micro-Channel for Refrigerant R134a," ASME Paper No. ICNMM2006-96211.
[17] Zhang, Y., Faghri, A., and Shafii, M. B., 2001, "Capillary Blocking in Forced Convective Condensation in Horizontal Miniature Channels," ASME J. Heat Transfer, **123**(3), pp. 501–511.
[18] Matkovic, M., Cavallini, A., Del Col, D., and Rossetto, L., 2009, "Experimental Study on Condensation Heat Transfer Inside a Single Circular Minichannel," Int. J. Heat Mass Transfer, **52**(9–10), pp. 2311–2323.
[19] Bonner, R. W., III, 2010, "Dropwise Condensation Life Testing of Self-Assembled Monolayers," ASME Paper No. IHTC14-22936.
[20] Ma, X., Wang, S., Lan, Z., Wang, A., and Peng, B., 2010, "Dropwise Condensation Heat Transfer on Superhydrophobic Surface in the Presence of Non-Condensable Gas," ASME Paper No. IHTC14-22248.
[21] Vemuri, S., and Kim, K., 2006, "An Experimental and Theoretical Study on the Concept of Dropwise Condensation," Int. J. Heat Mass Transfer, **49**(3–4), pp. 649–657.
[22] Haraguchi, T., Shimada, R., Kumagai, S., and Takeyama, T., 1991, "The Effect of Polyvinylidene Chloride Coating Thickness on Promotion of Dropwise Steam Condensation," Int. J. Heat Mass Transfer, **34**(12), pp. 3047–3054.
[23] Marto, P. J., Looney, D. J., Rose, J. W., and Wanniarachchi, A. S., 1986, "Evaluation of Organic Coatings for the Promotion of Dropwise Condensation of Steam," Int. J. Heat Mass Transfer, **29**(8), pp. 1109–1117.
[24] Das, A. K., Kilty, H. P., Marto, P. J., Andeen, G. B., and Kumar, A., 2000, "The Use of an Organic Self-Assembled Monolayer Coating to Promote Dropwise Condensation of Steam on Horizontal Tubes," ASME J. Heat Transfer, **122**(2), pp. 278–286.
[25] Dongchang, Z., Zaiqi, L., and Jifang, L., 1986, "New Surface Materials for Dropwise Condensation," 8th International Heat Transfer Conference, San Francisco, CA, Aug. 17–22, pp. 1677–1682.
[26] McNeil, D., Burnside, B., and Cuthbertson, G., 2000, "Dropwise Condensation of Steam on a Small Tube Bundle at Turbine Condenser Conditions," Exp. Heat Transfer, **13**(2), pp. 89–105.
[27] Ede, A. J., 2013, *An Introduction to Heat Transfer Principles and Calculations* (International Series of Monographs in Heating, Ventilation, and Refrigeration), Pergamon Press, Oxford, UK.
[28] Sommers, A. D., and Jacobi, A. M., 2006, "Creating Micro-Scale Surface Topology to Achieve Anisotropic Wettability on an Aluminum Surface," J. Micromech. Microeng., **16**(8), p. 1571.
[29] Abdelmessih, A. H., Neumann, A. W., and Yang, S. W., 1975, "The Effect of Surface Characteristics on Dropwise Condensation," Lett. Heat Mass Transfer, **2**(4), pp. 285–291.

[30] Cassie, A., and Baxter, S., 1944, "Wettability of Porous Surfaces," Trans. Faraday Soc., **40**, pp. 546–551.
[31] Wenzel, R. N., 1936, "Resistance of Solid Surfaces to Wetting by Water," Ind. Eng. Chem., **28**(8), pp. 988–994.
[32] Chen, X., Wu, J., Ma, R., Hua, M., Koratkar, N., Yao, S., and Wang, Z., 2011, "Nanograssed Micropyramidal Architectures for Continuous Dropwise Condensation," Adv. Funct. Mater., **21**(24), pp. 4617–4623.
[33] Enright, R., Miljkovic, N., Alvarado, J. L., Kim, K., and Rose, J. W., 2014, "Dropwise Condensation on Micro- and Nanostructured Surfaces," Nanoscale Microscale Thermophys. Eng., **18**(3), pp. 223–250.
[34] Lee, S., Cheng, K., Palmre, V., Bhuiya, M. D. M. H., Kim, K. J., Zhang, B. J., and Yoon, H., 2013, "Heat Transfer Measurement During Dropwise Condensation Using Micro/Nano-Scale Porous Surface," Int. J. Heat Mass Transfer, **65**, pp. 619–626.
[35] Lee, Y.-L., Fang, T.-H., Yang, Y.-M., and Maa, J.-R., 1998, "The Enhancement of Dropwise Condensation by Wettability Modification of Solid Surface," Int. Commun. Heat Mass Transfer, **25**(8), pp. 1095–1103.
[36] Bonner, R. W., 2010, "Dropwise Condensation Life Testing of Self-Assembled Monolayers," ASME Paper No. IHTC 14-22936.
[37] Das, A., Kilty, H., Marto, P., Andeen, G., and Kumar, A., 2000, "The Use of an Organic Self-Assembled Monolayer Coating to Promote Dropwise Condensation of Steam on Horizontal Tubes," ASME J. Heat Transfer, **122**(2), pp. 278–286.
[38] Cheng, L., Cheng, Y., Xin, G., and Zou, Y., 2010, "Influence of Ni-P Coating Microstructure on Condensation Heat Transfer," ASME Paper No. IHTC 14-22316.
[39] Depew, C. A., and Reisbig, R. L., 1964, "Vapor Condensation on a Horizontal Tube Using Teflon to Promote Dropwise Condensation," Ind. Eng. Chem. Process Des. Dev., **3**(4), pp. 365–369.
[40] Miljkovic, N., Enright, R., and Wang, E. N., 2012, "Effect of Droplet Morphology on Growth Dynamics and Heat Transfer During Condensation on Superhydrophobic Nanostructured Surfaces," ACS Nano, **6**(2), pp. 1776–1785.
[41] Miljkovic, N., Enright, R., and Wang, E. N., 2012, "Growth Dynamics During Dropwise Condensation on Nanostructured Superhydrophobic Surfaces," ASME Paper No. MNHMT2012-75278.
[42] Welch, J. F., 1961, "Microscopic Study of Dropwise Condensation," Ph.D. thesis, University of Illinois at Urbana-Champaign, Champaign, IL.
[43] Leach, R., Stevens, F., Langford, S., and Dickinson, J., 2006, "Dropwise Condensation: Experiments and Simulations of Nucleation and Growth of Water Drops in a Cooling System," Langmuir, **22**(21), pp. 8864–8872.
[44] Yamali, C., and Merte, H., Jr., 2002, "A Theory of Dropwise Condensation at Large Subcooling Including the Effect of the Sweeping," Heat Mass Transfer, **38**(3), pp. 191–202.
[45] McCormick, J. L., and Westwater, J. W., 1965, "Nucleation Sites for Dropwise Condensation," Chem. Eng. Sci., **20**(12), pp. 1021–1036.
[46] Rose, J., 1981, "Dropwise Condensation Theory," Int. J. Heat Mass Transfer, **24**(2), pp. 191–194.
[47] Rose, J., and Glicksman, L., 1973, "Dropwise Condensation—The Distribution of Drop Sizes," Int. J. Heat Mass Transfer, **16**(2), pp. 411–425.
[48] Dietz, C., Rykaczewski, K., Fedorov, A. G., and Joshi, Y., 2010, "Visualization of Droplet Departure on a Superhydrophobic Surface and Implications to Heat Transfer Enhancement During Dropwise Condensation," Appl. Phys. Lett., **97**(3), p. 033104.
[49] Webb, R. L., 1994, *Principles of Enhanced Heat Transfer*, Wiley, New York.
[50] Fang, C., Steinbrenner, J. E., Wang, F.-M., and Goodson, K. E., 2010, "Impact of Wall Hydrophobicity on Condensation Flow and Heat Transfer in Silicon Microchannels," J. Micromech. Microeng., **20**(4), p. 045018.
[51] Derby, M. M., Chatterjee, A., Peles, Y., and Jensen, M. K., 2014, "Flow Condensation Heat Transfer Enhancement in a Mini-Channel With Hydrophobic and Hydrophilic Patterns," Int. J. Heat Mass Transfer, **68**, pp. 151–160.
[52] Garimella, S., 2003, "Condensation Flow Mechanisms in Microchannels: Basis for Pressure Drop and Heat Transfer Models," ASME Paper No. ICMM2003-1020.
[53] Thome, J., Bar-Cohen, A., Revellin, R., and Zun, I., 2013, "Unified Mechanistic Multiscale Mapping of Two-Phase Flow Patterns in Microchannels," Exp. Therm. Fluid Sci., **44**, pp. 1–22.
[54] Kim, S. M., and Mudawar, I., 2013, "Universal Approach to Predicting Heat Transfer Coefficient for Condensing Mini/Micro-Channel Flow," Int. J. Heat Mass Transfer, **56**(1–2), pp. 238–250.
[55] Chen, Y., Wu, R., Shi, M., Wu, J., and Peterson, G. P., 2009, "Visualization Study of Steam Condensation in Triangular Microchannels," Int. J. Heat Mass Transfer, **52**(21–22), pp. 5122–5129.
[56] Liebenberg, L., Thome, J. R., and Meyer, J. P., 2005, "Flow Visualization and Flow Pattern Identification With Power Spectral Density Distributions of Pressure Traces During Refrigerant Condensation in Smooth and Microfin Tubes," ASME J. Heat Transfer, **127**(3), pp. 209–220.
[57] Chen, X., and Derby, M. M., 2015, "Visualization of Steam Flow Condensation in Hydrophobic and Hydrophilic Mini-Gaps," ASME Paper No. IMECE2015-51150.
[58] Lockhart, R., and Martinelli, R., 1949, "Proposed Correlation of Data for Isothermal Two-Phase, Two-Component Flow in Pipes," Chem. Eng. Prog., **45**(1), pp. 39–48.
[59] Kim, S. M., and Mudawar, I., 2014, "Review of Databases and Predictive Methods for Pressure Drop in Adiabatic, Condensing and Boiling Mini/Micro-Channel Flows," Int. J. Heat Mass Transfer, **77**, pp. 74–97.
[60] Kedzierski, M., and Worthington, J., III, 1993, "Design and Machining of Copper Specimens With Micro Holes for Accurate Heat Transfer Measurements," Exp. Heat Transfer, **6**(4), pp. 329–344.
[61] Kline, S. J., and McClintock, F., 1953, "Describing Uncertainties in Single-Sample Experiments," ASME Mech. Eng., **75**(1), pp. 3–8.
[62] Wang, H. S., and Rose, J. W., 2006, "Film Condensation in Microchannels: Effect of Tube Inclination," Fourth International Conference on Nanochannels, Microchannels and Minichannels, pp. 133–137.
[63] Wang, H. S., and Rose, J. W., 2005, "A Theory of Film Condensation in Horizontal Noncircular Section Microchannels," ASME J. Heat Transfer, **127**(10), p. 1096.
[64] Agarwal, A., Bandhauer, T. M., and Garimella, S., 2007, "Heat Transfer Model for Condensation in Non-Circular Microchannels," Fifth International Conference on Nanochannels, Microchannels, and Minichannels, Puebla, Mexico, pp. 117–126.
[65] Derby, M. M., Lee, H. J., Peles, Y., and Jensen, M. K., 2012, "Condensation Heat Transfer in Square, Triangular, and Semi-Circular Mini-Channels," Int. J. Heat Mass Transfer, **55**(1–3), pp. 187–197.
[66] Marto, P., Looney, D., Rose, J., and Wanniarachchi, A., 1986, "Evaluation of Organic Coatings for the Promotion of Dropwise Condensation of Steam," Int. J. Heat Mass Transfer, **29**(8), pp. 1109–1117.
[67] Rose, J., 1998, "Condensation Heat Transfer Fundamentals," Chem. Eng. Res. Des., **76**(2), pp. 143–152.